Open Access

Earth System
Science
Data

Radiocarbon measurements of ecosystem respiration and soil pore-space CO$_2$ in Utqiaġvik (Barrow), Alaska

Lydia J. S. Vaughn[1,2] **and Margaret S. Torn**[2,3]

[1]Integrative Biology, University of California, Berkeley, Berkeley, CA 94720, USA
[2]Lawrence Berkeley National Laboratory, Berkeley, CA 94720, USA
[3]Energy and Resources Group, University of California, Berkeley, Berkeley, CA 94720, USA

Correspondence: Lydia J. S. Vaughn (lydiajsvaughn@gmail.com)

Abstract. Radiocarbon measurements of ecosystem respiration and soil pore space CO$_2$ are useful for determining the sources of ecosystem respiration, identifying environmental controls on soil carbon cycling rates, and parameterizing and evaluating models of the carbon cycle. We measured flux rates and radiocarbon content of ecosystem respiration, as well as radiocarbon in soil profile CO$_2$ in Utqiaġvik (Barrow), Alaska, during the summers of 2012, 2013, and 2014. We found that radiocarbon in ecosystem respiration ($\Delta^{14}C_{Reco}$) ranged from $+60.5$ to -160‰ with a median value of $+23.3$‰. Ecosystem respiration became more depleted in radiocarbon from summer to autumn, indicating increased decomposition of old soil organic carbon and/or decreased CO$_2$ production from fast-cycling carbon pools. Across permafrost features, ecosystem respiration from high-centered polygons was depleted in radiocarbon relative to other polygon types. Radiocarbon content in soil pore-space CO$_2$ varied between -7.1 and -280‰, becoming more negative with depth in individual soil profiles. These pore-space radiocarbon values correspond to CO$_2$ mean ages of 410 to 3350 years, based on a steady-state, one-pool model. Together, these data indicate that deep soil respiration was derived primarily from old, slow-cycling carbon, but that total CO$_2$ fluxes depended largely on autotrophic respiration and heterotrophic decomposition of fast-cycling carbon within the shallowest soil layers. The relative contributions of these different CO$_2$ sources were highly variable across microtopographic features and time in the sampling season. The highly negative $\Delta^{14}C$ values in soil pore-space CO$_2$ and autumn ecosystem respiration indicate that when it is not frozen, very old soil carbon is vulnerable to decomposition. Radiocarbon data and associated CO$_2$ flux and temperature data are stored in the data repository of the Next Generation Ecosystem Experiments (NGEE-Arctic) at http://dx.doi.org/10.5440/1364062 and https://doi.org/10.5440/1418853.

1 Introduction

The flux of CO$_2$ from ecosystems to the atmosphere is a critical component of the global carbon budget. This flux is highly heterogeneous in space and time, so extensive datasets are needed to evaluate the carbon balance within ecosystems. Many measurements have been made of soil surface CO$_2$ emissions using soil chambers and eddy covariance towers (e.g., Baldocchi, 2008; Bond-Lamberty and Thomson, 2010; Davidson et al., 2002; Norman et al., 1997; Xu and Baldocchi, 2004). Such measurements reveal spatial and temporal patterns in soil and ecosystem respiration that are im-

portant for scaling soil carbon emissions across the landscape or identifying drivers of respiration rates (Wainwright et al., 2015). Bulk fluxes of soil or ecosystem respiration, however, do not provide information on the cycling rates or relative contributions of different soil carbon pools to total CO$_2$ emissions. CO$_2$ emitted from the soil surface includes autotrophic respiration of rapidly cycling carbon as well as heterotrophic decomposition of carbon that cycles on a broad range of timescales. Shifts in these carbon pool distributions can have large long-term consequences for soil carbon stocks, but may be impossible to detect in bulk CO$_2$

flux rates (Hopkins et al., 2012; Schuur et al., 2009; Torn et al., 2009; Trumbore, 2000, 2009).

Linking CO_2 emissions with carbon cycling rates requires a tracer of carbon dynamics that can differentiate between source carbon pools. Natural abundance radiocarbon provides such a tracer, as the radiocarbon content of CO_2 reflects the age (since photosynthesis) and decomposition rates of its component sources (Trumbore, 2000). Accordingly, radiocarbon in surface CO_2 emissions and soil pore gas can be used to quantify carbon cycling rates and assess their variability across space, time, carbon pools, and environmental factors such as soil moisture, temperature, and vegetation (Gaudinski et al., 2000; Trumbore, 2000). Within and across sites, variations in the radiocarbon abundance of respired CO_2 can indicate differences in substrate utilization by microbial decomposers (Borken et al., 2006; Chasar et al., 2000) and shifts between more fast-cycling and slow-cycling substrates (Hicks Pries et al., 2013; Hopkins et al., 2012; Schuur et al., 2009). Radiocarbon measurements of soil respiration may be particularly useful for models of the carbon cycle. Carbon pool structures and decomposition dynamics inferred from radiocarbon data may be used to parameterize pool-specific respiration rates; radiocarbon measurements in surface CO_2 emissions and soil pore gas can be used to benchmark model performance; and the radiocarbon signature of respiration can be used to constrain the terrestrial signal in top-down carbon cycle analyses (He et al., 2016; Randerson et al., 2002).

In the high latitudes in particular, increased decomposition rates from large, slow-cycling soil carbon stores have the potential to generate an important long-term climate change feedback (Schuur et al., 2015). There, an estimated 1300 Pg of soil carbon has been protected from decomposition by cold temperatures and often frozen or anoxic conditions (Hugelius et al., 2014). With climate change, these controls on decomposition rates are expected to change as soils warm, hydrological changes occur, and permafrost degradation intensifies (ACIA, 2004). In the lower depths of the seasonally thawed active layer, carbon that has historically cycled on millennial timescales may be highly decomposable under aerobic and thawed conditions (Elberling et al., 2013; Mueller et al., 2015; Strauss et al., 2015; Waldrop et al., 2010). Our current understanding of this old carbon's decomposability, however, is based primarily on CO_2 production rates from laboratory incubations, which may not accurately reflect in situ decomposition dynamics. To quantify in situ decomposition rates, field radiocarbon measurements can be used to differentiate between slow-cycling and fast-cycling carbon and link decomposition dynamics to their environmental controls.

In spite of their use in tracing carbon cycle dynamics, only a limited set of radiocarbon data have been published for Arctic ecosystem respiration (e.g., Hardie et al., 2009; Hicks Pries et al., 2013; Lupascu et al., 2014a; Nowinski et al., 2010; Phillips et al., 2015; Schuur et al., 2009) or
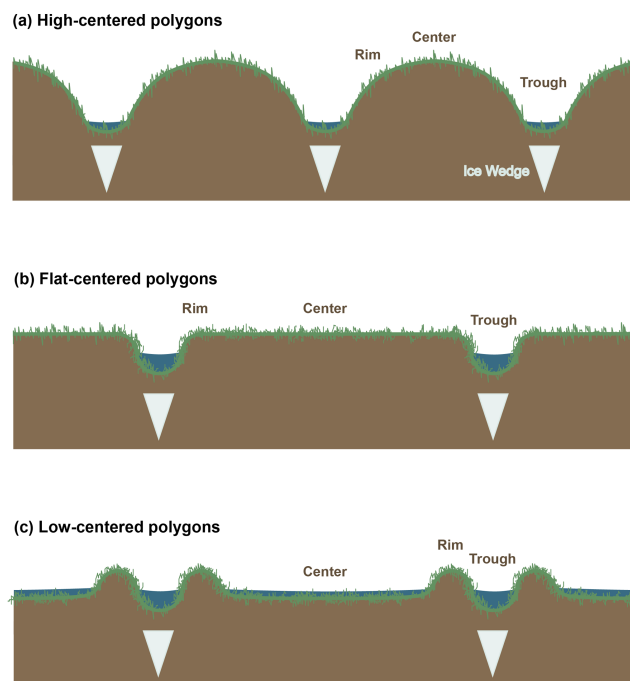

Figure 1. Schematic diagram of polygon morphology. Ice wedge locations and the relative scales of features are approximate.

soil pore-space CO_2 (Czimczik and Welker, 2010; Lupascu et al., 2014a, b), from only a few sites and tundra types. To our knowledge, no data are currently available on radiocarbon in CO_2 from Arctic polygon tundra. Polygon tundra, which covers an estimated $250\,000\,\mathrm{km}^2$ throughout the Arctic (Donner et al., 2007), is characterized by microtopographic features ~ 10–$32\,\mathrm{m}$ in diameter known as ice wedge polygons, which form by the growth and subsequent degradation of subsurface ice formations (ice wedges) (Billings and Peterson, 1980; Brown et al., 1980). Polygons are separated by low-lying drainage channels called troughs, and can be classified according to the elevation of their centers into low-centered, flat-centered, and high-centered categories. Low-centered polygons (LC) have raised, dry rims at their perimeter surrounding low, saturated or inundated centers; flat-centered polygons (FC) have flat, even surfaces with minimal rim delineation; and high-centered polygons (HC) have raised centers with dry surface soils that slope steeply into troughs (Fig. 1). Among LC, FC, and HC polygons, differences in active layer depth, oxygen availability, soil carbon distribution, and thermal conductivity (Liljedahl et al., 2016; Lipson et al., 2012; Ping et al., 1998) create strong differences in surface carbon fluxes (Vaughn et al., 2016; Wainwright et al., 2015). Given these steep spatial gradients in carbon cycling rates and their environmental controls, radiocarbon in respiration from polygon tundra ecosystems offers unique information on subsurface carbon

dynamics across space, environmental factors, and the progression of seasonal thaw.

Here, we present measurements of radiocarbon in ecosystem respiration, soil pore-space CO$_2$, and soil organic carbon from a polygon tundra ecosystem in Utqiaġvik, Alaska. We measured rates and radiocarbon contents of soil surface CO$_2$ emissions across three summer seasons, from a range of ice wedge polygon features. Using soil pore-space ^{14}CO$_2$ profiles, we quantified vertical distributions of carbon cycling rates within the soil profile. Together, these measurements reveal temporal patterns and spatial relationships in ecosystem respiration and its source carbon pools.

2 Study site

Field sampling was conducted at the Barrow Environmental Observatory (BEO), ~ 6 km east of Utqiaġvik (formerly Barrow), Alaska (71.3° N, 156.5° W), at the northern end of the Alaskan Arctic coastal plain. Utqiaġvik has a mean annual temperature of -9.8 °C and mean annual precipitation of 146 mm, with long, dry winters and short, moist, cool summers (NOAA, 2018). The land surface has low topographic relief reaching a maximum elevation of 5 m (Brown et al., 1980; Hubbard et al., 2013). The seasonally thawed active layer ranges in depth from 20 to 60 cm, underlain by continuous ice-rich permafrost to depths greater than 400 m (Hinkel and Nelson, 2003). Formed from the late Pleistocene Gubic formation (Black, 1964), soils in the region are dominated by Typic Aquiturbels (53 %), Typic Histoturbels (22 %), and Typic Aquorthels (8.6 %) (Bockheim et al., 1999). Across the Utqiaġvik peninsula, 24 % of the ground surface is covered by LC polygons, 17 % by FC polygons, 11 % by HC polygons, and 5 % by their surrounding troughs (Lara et al., 2014). Within the specific study region, polygons cover the majority of the land surface, with the remainder comprised of a polygon-free drainage region. In the study area, FC polygons occupy the greatest percentage of the total ground surface, HC polygons occupy the smallest percentage, and LC polygons have intermediate percentage cover (Wainwright et al., 2015). Sample collection was distributed across centers, rims, and troughs of the three polygon types to capture variations in polygon microtopography and associated carbon cycle controls.

3 Field measurements and sample collection

3.1 Surface CO$_2$ emissions

In August and October 2012, July and September 2013, and September 2014, we collected soil surface CO$_2$ emissions for radiocarbon analysis using a static chamber method modified from Hahn et al. (2006). Samples were collected from a total of 19 locations within 11 polygons (4 LC, 4 FC, 3 HC). Opaque chambers (25 cm diameter) were seated on circular PVC chamber bases extending to depths of ~ 10 cm

below the soil surface, with aboveground chamber height varying between ~ 15 and 20 cm. We installed all bases at least 2 days prior to sampling to limit the influence of disturbance on gas flux rates and radiocarbon values. Chambers blocked light transmission and were tall enough to enclose surface vegetation, so CO$_2$ emissions were equivalent to ecosystem respiration. For sample collection, the chamber was placed in a 3 cm deep channel on the top rim of each base, which was filled with water to create an airtight seal. We then circulated chamber gas through soda lime for 20 min at a flow rate of 1 L min^{-1} to remove ambient CO$_2$. CO$_2$ was allowed to accumulate in the chamber over 2 to 48 h, depending on the rate of CO$_2$ accumulation, which we monitored periodically by injecting a 30 mL sample of chamber gas into a LI-820 CO$_2$ gas analyzer (LI-COR) at a flow rate of ~ 1 L min^{-1}. For all samples, the final chamber CO$_2$ concentration was more than twice its initial concentration, important for accuracy in chamber radiocarbon measurements (Egan et al., 2014). Based on this concentration measurement, a volume of chamber gas sufficient for radiocarbon analysis was collected in one or more 500–1000 mL evacuated stainless steel canisters connected by capillary tubing to a chamber sampling port. High-concentration samples were collected with a syringe and needle through a septum in the sampling port and immediately injected into evacuated glass vials sealed with 14 mm thick chlorobutyl septa (Bellco Glass, Inc.). To correct chamber gas samples for atmospheric contamination, we collected local air samples in 3000 mL stainless steel canisters on 12 August 2012, 13 July 2013, and 2 and 7 September 2014.

In July and September 2013 and September 2014, we measured rates of ecosystem respiration from radiocarbon sampling locations. CO$_2$ fluxes were measured within 2 days of radiocarbon sample collection, using opaque static chambers seated on bases described above and vented according to Xu et al. (2006) to minimize pressure changes due to the Venturi effect. For each measurement, we measured CO$_2$ concentrations within the chamber over a period of 4–8 min using a Los Gatos Research, Inc. Portable Greenhouse Gas Analyzer. We calculated the CO$_2$ flux rate (equivalent to ecosystem respiration) as the slope of the linear portion of its concentration vs. time curve, converted to units of μmol m^{-2} s^{-2} according to chamber volume and temperature. Endpoints of this linear region were determined manually for each curve, and curves lacking a clear linear range were not included in the dataset. Corresponding to each CO$_2$ flux measurement, we measured thaw depth with a tile probe.

3.2 Soil pore-space CO$_2$

In August 2012 and July 2013, we collected soil pore gas from a total of six soil profiles within five polygons (one LC, two FC, two HC). Samples were collected with a method similar to Czimczik and Welker (2010). Briefly, 1/4″ diameter stainless steel probes were inserted into the soil at 45° an-

gles to vertical depths of 10, 20, and 30 cm, or to 2 cm above the frost table if thaw depth was less than 30 cm. Probes were capped with gastight septa and allowed to remain in place throughout the sampling season. Before collecting each sample, we purged 10 mL of gas from the probe and measured the CO_2 concentration with a LI-820 CO_2 gas analyzer as described above. Radiocarbon samples were collected by connecting evacuated 500–1000 mL stainless steel canisters to probes via flow-restricting tubing (Upchurch scientific, 0.01″ ID ×10 cm length), which allowed canisters to fill slowly over 4 h with minimal disturbance to the soil CO_2 concentration gradient (Gaudinski et al., 2000). In-line Drierite water traps were used during sample collection to prevent moisture accumulation in canisters. As with surface respiration samples, high-concentration samples were collected from probes with a syringe and needle and immediately injected into evacuated glass vials. Due to water-saturated soils or clogged soil probes, we were unable to obtain samples from all profiles and depths. For this reason, the final sample set represents only a subset of depths and sampling locations and is not a random sample of the entire landscape.

3.3 Soil organic matter

On 8 September 2014, we collected 1″ diameter soil cores from the centers of the nine polygons used for September 2014 soil surface CO_2 sampling (3 LC, 3 FC, 3 HC). Soil cores were collected from within 0.5 m of each static chamber. Cores were collected using a manual soil recovery probe (AMS Samplers Inc.) to the base of the thawed soil layer (16–44 cm depth) and stored intact for 8 days at 5 °C before further processing. Following this 8-day period, cores from FC and HC polygons were divided into 2 equal depth increments, which ranged from 8 to 15.5 cm in length. In the case of LC polygons, where standing water was present at the time of sampling, the shallow and deep increments were defined as surface water and sediment, respectively. For a separate experiment, core increments were incubated at 3 °C for 387 days, during which CO_2 production rates were monitored with a LI-820 CO_2 analyzer (LI-COR). Following this 387-day period, we collected evolved CO_2 for radiocarbon analysis using stainless steel air sampling canisters or glass serum vials. Incubated soil, water, and sediment samples were freeze-dried and ground for carbon content and radiocarbon analyses.

3.4 Sample purification and radiocarbon analysis

CO_2 from gas samples was cryogenically purified under vacuum, divided for ^{14}C and ^{13}C analysis, and sealed in 9 mm quartz tubes. For radiocarbon analysis, we sent samples to Lawrence Livermore National Laboratory's Center for Accelerator Mass Spectrometry (CAMS) or the Carbon, Water, and Soils Research Lab at the USDA-FS Northern Research Station, where CO_2 was reduced to graphite on iron powder

under H$_2$. ^{14}C abundance was then measured at CAMS using an HVEC FN Tandem Van de Graaff accelerator mass spectrometer or at UC Irvine's Keck Carbon Cycle AMS facility. ^{13}C/^{12}C in CO_2 splits was analyzed on the UC Davis Stable Isotope Laboratory GVI Optima Stable Isotope Ratio Mass Spectrometer.

Two quality control measures were employed to test for contamination by non-sample carbon during gas sample storage and preparation. First, we evaluated the air sampling canisters with repeated leak testing and an ethanol-derived certified CO_2 reference gas standard with empirically determined ^{14}C (Airgas, USA) to confirm that no contamination was introduced during sample storage. Second, the vacuum line used for CO_2 purification was tested with USGS coal and oxalic acid II (NIST SRM 4990C) standards for contamination or leakage. Standards were well characterized with respect to ^{14}C.

Subsamples of bulk soil from the 2014 incubation were sent to the Carbon, Water, and Soils Research Lab, where they were combusted to CO_2 and analyzed for radiocarbon as above. Carbon concentrations and ^{13}C abundances were measured on a Costech analytical Technologies ECS 4010 elemental analyzer coupled to a Thermo Fischer Scientific Delta V^{plus} isotope ratio mass spectrometer. Given the acidic pH range of soils at this site (Zona et al., 2011), we consider bulk soil carbon to be equivalent to soil organic carbon.

Following the conventions of Stuiver and Polach (1977), radiocarbon results are presented as fraction modern relative to the NBS Oxalic Acid I (OX1) standard (F^{14}C), and deviations in parts per thousand (‰) from the absolute (decay-corrected) OX1 standard (Δ^{14}C). All results have been corrected for mass-dependent isotopic fractionation using ^{13}C measurements.

4 Calculations and data quality control

4.1 Correction of surface CO_2 emissions for atmospheric contamination

We corrected surface-chamber radiocarbon measurements for atmospheric contamination using the method described in Schuur and Trumbore (2006). Briefly, we determined fractional contributions of background atmosphere and ecosystem respiration to total chamber gas using ^{13}C values in a two-pool mixing model:

$$^{13}C_S = f_{Reco} \times {}^{13}C_{Reco} + f_{atm} \times {}^{13}C_{atm}, \tag{1}$$

$$f_{Reco} + f_{atm} = 1, \tag{2}$$

where f_{Reco} and f_{atm} are the fractional contributions of ecosystem respiration and background atmosphere, $^{13}C_S$ and $^{13}C_{atm}$ are the measured ^{13}C abundances in the sample and background atmosphere in units of at. %, and $^{13}C_{Reco}$ is the ^{13}C abundance in ecosystem respiration, approximated separately for each polygon type as the mean ^{13}C of chamber

CO$_2$ samples with [CO$_2$] > 4000 ppm. Mean $\delta^{13}C_{Reco}$ values calculated this way were -24.6, -26.5, and $-26.2\%o$ for LC, FC, and HC polygons. To minimize error due to large proportions of atmospheric CO_2, we omitted samples with $f_{Reco} < 0.5$. For each sample, we calculated $\Delta^{14}C$ of ecosystem respiration ($\Delta^{14}C_{Reco}$) according to Eq. (3):

$$\Delta^{14}C_S = f_{Reco} \times \Delta^{14}C_{Reco} + f_{atm} \times \Delta^{14}C_{atm}, \qquad (3)$$

where $\Delta^{14}C_S$ and $\Delta^{14}C_{atm}$ are the measured $\Delta^{14}C$ values of the sample and background atmosphere, and f_{Reco} and f_{atm} were calculated from Eqs. (1) and (2). Errors due to analytical precision and variations in source isotopic signatures were propagated through this correction according to the formulation in Phillips and Gregg (2001).

Soil surface CO_2 flux measurements were assessed for quality using two criteria, the standard error of the slope (SE) and the per cent relative standard error (PRSE), defined as $100 \times SE_{slope}/Estimate_{slope}$. Flux measurements with SE > 0.05 and PRSE > 5 were omitted from the dataset. This set of dual criteria avoided biasing the dataset toward low fluxes (if SE alone were used) or high fluxes (if PRSE alone or R^2 were used).

4.2 Modeled mean age of soil pore-space CO_2

With soil pore-space radiocarbon data, we omitted measurements with CO_2 yields below the expected yield for atmospheric measurements due to possible leakage and atmospheric contamination during sampling, with the exception of one sample from 31 cm depth with highly negative $\Delta^{14}C$, indicating a low proportion of atmospheric CO_2. At this field site, ^{13}C abundances in pore-space CO_2 vary greatly due to isotopic fractionation from methane production and consumption (Vaughn et al., 2016). For this reason, we could not correct subsurface samples for atmospheric CO_2. Reported radiocarbon values thus represent the total CO_2 present in the soil pore space, sourced from heterotrophic respiration, root respiration, and downward atmospheric diffusion.

With soil-profile CO_2 samples, we used radiocarbon measurements to model the mean age of carbon in respired CO_2 using the time-dependent steady-state turnover time model described in Torn et al. (2009), modified to account for carbon residence time in plant tissues:

$$F'_{C,t} C_t = I F'_{atm, t-T_R} + C_{t-1} F'_{C,t-1} \left(1 - \frac{1}{\tau} - \lambda\right), \qquad (4)$$

where $F' = \frac{\Delta^{14}C}{1000} - 1$, $F'_C = F'$ of the given carbon pool, equal to F' of the CO_2 sample, $F'_{atm} = F'$ of CO_2 in the local atmosphere, $I =$ input rate of carbon from the atmosphere to the given carbon pool (g C y^{-1}), $C =$ stock of carbon in the given carbon pool (g), $\tau =$ turnover time of the given carbon pool, equivalent to the mean age of carbon in its decomposition flux (y) at steady state, $\lambda =$ radioactive decay rate of

^{14}C (1/8267 y), and $T_R =$ mean residence time of carbon in plants before entering soil organic matter (y).

At steady state, $C_t = C_{t-1} = I \times \tau$, so Eq. (4) reduces to

$$F'_{C,t} = \frac{1}{\tau} F'_{atm, t-T_R} + F'_{C, t-1} \left(1 - \frac{1}{\tau} - \lambda\right). \qquad (5)$$

Following Eq. (5), the $\Delta^{14}C$ value of CO_2 at time t thus depends on the turnover time of carbon in the decomposing carbon pool, the mean residence time of carbon in plant material, and the $\Delta^{14}C$ of atmospheric CO_2 in the current and previous years, which has changed continuously since the release of radiocarbon into the atmosphere from nuclear weapons testing between 1950 and the mid 1960s (Trumbore, 2000). This model assumes that CO_2 is derived from a homogeneous pool of decomposing carbon, such that the turnover time of this pool is equal to the mean age of its decomposition flux at steady state (Sierra et al., 2017).

The mean residence time of carbon in plants (T_R) reflects a mixture of materials with varying transfer rates. In the Arctic vegetation dominant at our site, some photosynthates enter the soil within 1 day of fixation (Loya et al., 2002); leaf tissues with transit times of < 1 year represent the majority of annual production (Shaver and Kummerow, 1991); roots and shoots are estimated to live for ranges of 3–7 and 1–8 years, respectively (Chapin III et al., 1980; Shaver and Billings, 1975), and rhizomes and stem bases, the longest-lived of belowground tissues, have estimated lifetimes of 2.7–15.6 years (Dennis, 1977). Overall, T_R represents the flux-weighted average of these various pools. Given the large percentage of carbon flux dedicated to annual leaf production and rapid transport to soils, we estimate that across plant organs, plant species, and seasons, the mean value of T_R lies between 0 and 5 years.

Annual atmospheric $\Delta^{14}C$ values were compiled from our data and three other sources: the IntCal13 dataset (Reimer et al., 2013), measurements from Fruholmen, Norway, between 1962 and 1991 (Nydal and Lövseth, 1996), measurements from Utqiaġvik between 1999 and 2007 (Graven et al., 2012), and our measurements from the BEO in 2012, 2013, and 2014. From roughly the same latitude as Utqiaġvik, Fruholmen $\Delta^{14}C$ measurements provide a close approximation for missing Utqiaġvik data (Meijer et al., 2008). Because ecosystem CO_2 uptake occurs primarily during the growing season, we averaged June–August $\Delta^{14}C$ values to produce an annualized summer dataset. Data gaps from 1992–1998 and 2008–2011 were filled using an exponential interpolation constrained by the available data from the 10 years surrounding each gap.

Using our measured $\Delta^{14}C$ values and annually resolved atmospheric $\Delta^{14}C$ data, we iteratively solved for the mean age of each CO_2 sample. We performed this calculation twice, using T_R values of 0 and 5 to bracket the likely T_R range. Samples containing a large percentage of recently fixed carbon yielded two possible solutions for each T_R value

(Trumbore, 2000). In such cases, we chose the appropriate solution either by comparing the two values to other (unique) mean age values within the same profile, or by comparing the measured carbon stock with the carbon stocks calculated from the CO_2 production rate and the candidate solutions (Torn et al., 2009).

4.3 Correction of soil organic carbon for respiration losses

To calculate $\Delta^{14}C$ values of soil organic carbon, we corrected bulk soil $\Delta^{14}C$ measurements for loss of CO_2 respired during the 387-day incubation. We used the post-incubation masses of non-respired soil carbon (C_{soil}, calculated from measured soil carbon contents and sample masses) and carbon respired as CO_2 (C_{CO_2}, calculated from CO_2 production rates) to calculate pre-incubation $\Delta^{14}C$ values of bulk soil organic carbon ($\Delta^{14}C_{SOC}$) according to

$$\Delta^{14}C_{SOC} = \frac{C_{soil}}{C_{soil} + C_{CO_2}} \times \Delta^{14}C_{soil} + \frac{C_{CO_2}}{C_{soil} + C_{CO_2}} \times \Delta^{14}C_{CO_2}, \tag{6}$$

where $\Delta^{14}C_{soil}$ and $\Delta^{14}C_{CO_2}$ are the radiocarbon abundances measured from bulk soil and respired CO_2 following the incubation.

5 Results and discussion

5.1 Radiocarbon in ecosystem respiration

Radiocarbon contents of soil surface CO_2 emissions, equivalent to ecosystem respiration ($\Delta^{14}C_{Reco}$), ranged from $+60.5$ to $-160\%o$, with a median value of $+23.3\%o$ (Table S1 in the Supplement). The positive $\Delta^{14}C_{Reco}$ values measured in 28 of the 37 samples indicate high proportions of carbon fixed since 1950, likely sourced from both autotrophic respiration and decomposition of rapidly cycling soil carbon in shallow soil layers. In contrast, the negative values measured in the other nine samples show that the sources of CO_2 at those times and places were dominated by carbon that cycles on centennial to millennial timescales. $\Delta^{14}C_{Reco}$ followed a left-skewed distribution, with notably negative $\Delta^{14}C_{Reco}$ values measured from LC1-center in October 2012 ($-159.5\%o$) and HC1-center in September 2013 ($-115.5\%o$). The variations in these $\Delta^{14}C_{Reco}$ values reflect differences in the relative CO_2 production and transport rates from both autotrophic and heterotrophic source pools, whose decomposition rates and radiocarbon contents vary spatially and temporally (Nowinski et al., 2010). Together, seasonal variations in soil thaw depths and spatial variations in soil organic carbon ^{14}C depth profiles are known to affect the radiocarbon signature of surface CO_2 emissions.

From data compiled over the 3 measurement years, the lowest $\Delta^{14}C_{Reco}$ values were measured in September, when
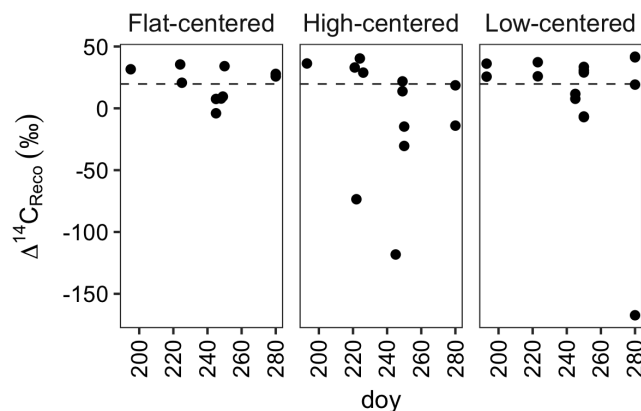

Figure 2. Radiocarbon content of ecosystem respiration, sampled from flat-centered, high-centered, and low-centered polygons in 2012, 2013, and 2014. All samples have been corrected for atmospheric contamination using ^{13}C and ^{14}C abundances of the local atmosphere at the time of sample collection. Dashed horizontal line indicates the mean $\Delta^{14}C$ of local atmospheric CO_2 during the 2012–2014 summer seasons.

the depth of soil thaw was near its annual maximum (Fig. 2). This observation is consistent with other data from high-latitude sites (Hicks Pries et al., 2013; Trumbore, 2000) and reflects seasonal changes in thaw depth, soil temperature, and vegetation activity. Surface soils at this site begin to thaw in June, typically reaching their maximum temperatures in July (Hinkel et al., 2001; Torn, 2015). As shallow soils warm and plant activity increases in this early summer period, ecosystem respiration includes high proportions of ^{14}C-enriched CO_2 from autotrophic respiration and heterotrophic decomposition of shallow, rapid-cycling soil carbon (Fig. 2). Autotrophic respiration peaks in July or August, and decreases substantially into the fall after plants senesce (Hicks Pries et al., 2013), shifting the balance of respiration toward soil carbon decomposition. As thaw depth increases into October (Table S1) (Zona et al., 2016), decomposition of deep, ^{14}C-depleted soil carbon can become an increasing fraction of total soil respiration. The effect of these changes is a seasonal shift in respiration from primarily shallow, fast-cycling source carbon pools to deeper, more ^{14}C-depleted soil organic matter.

Whereas September $\Delta^{14}C_{Reco}$ values were notably low, this was not the case with October measurements (Fig. 2). Although it is possible that this observation reflects the relative carbon mineralization rates of the different soil depths, the relatively enriched $\Delta^{14}C_{Reco}$ values measured in October may instead be due to physical limitations to gas transport within the soil profile or bias in the distribution of samples across polygon types and features. Surface soils were frozen at the time of October sample collection, possibly trapping deeper, ^{14}C-depleted CO_2 below the surface soil layers. This effect has been proposed as a mechanism underlying pulses
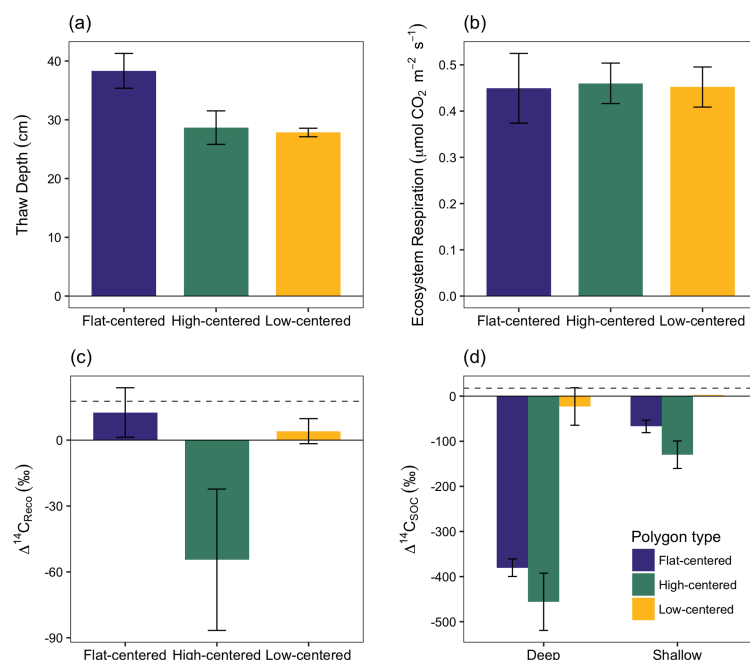
Figure 3. Depth of soil thaw **(a)**, ecosystem respiration rate **(b)**, radiocarbon content of ecosystem respiration **(c)**, and radiocarbon content of bulk soil organic carbon **(d)**, measured from polygon centers in September 2014. Error bars represent standard error with $n = 3$ with the exception of $\Delta^{14}C_{SOC}$ from shallow low-centered polygons ($n = 2$; no standard error calculated). Dashed horizontal line indicates $\Delta^{14}C$ of local atmospheric CO_2 at the time of sampling. In panel **(d)**, deep and shallow samples represent the lower and upper halves of the thawed soil layer for flat-centered and high-centered polygons. For low-centered polygons, shallow samples were collected as standing water and deep samples span the full depth of the thawed sediment layer.

of CO_2 release during the autumn freeze-up and spring thaw periods (Bubier et al., 2002; Oechel et al., 1997; Raz-Yaseef et al., 2017). In the absence of such a pulse, surface CO_2 fluxes may be derived largely from shallow soil decomposition, yielding relatively enriched $\Delta^{14}C_{Reco}$ values late in the autumn season. Additionally, because of snow and frozen surface soils, we were unable to obtain CO_2 samples from a number of locations. Notably, measurements from the centers of HC and FC polygons are absent from the October dataset. If the seasonal decrease in $\Delta^{14}C_{Reco}$ were greatest in polygon centers, the lack of ^{14}C-depleted October measurements may thus be due to this sampling bias.

Time-series measurements from individual profiles or polygon types indicate that $\Delta^{14}C_{Reco}$ varied not only with time in the sampling season, but also with polygon type (Fig. 2, Table S1). HC polygons displayed particularly strong seasonal trends in $\Delta^{14}C_{Reco}$; in each HC polygon from which multiple measurements were made, $\Delta^{14}C_{Reco}$ decreased throughout the summer months to a minimum value in September or October. The magnitude of this seasonal decrease varied greatly among individual HC polygons and microtopographic positions within the polygons, reaching a minimum $\Delta^{14}C_{Reco}$ value of $-115\,‰$ from the center of polygon HC1, but only $+13\,‰$ from the trough of HC3 (Table S1). In contrast with HC polygons, $\Delta^{14}C_{Reco}$ from

FC and LC polygons remained closer to atmospheric values throughout the sampling season (Fig. 2). One exception was one highly negative $\Delta^{14}C_{Reco}$ value measured in October from the center of polygon LC1. In this instance, with October thaw depths close to their annual maximum (Zona et al., 2016), thaw may have penetrated into the transition layer at the top of the permafrost, exposing old, previously frozen carbon to decomposition. Alternatively, this isolated measurement of ^{14}C-depleted CO_2 may reflect heterogeneity within the active layer due to cryoturbation, the vertical transport of soil material due to freeze–thaw processes (Kaiser et al., 2007; Ping et al., 1998).

In September 2014, we measured $\Delta^{14}C_{Reco}$, $\Delta^{14}C_{SOC}$, and ecosystem respiration rates from the centers of three polygons of each type (Fig. 3, Table S2). The influence of microtopography on old carbon emissions was particularly apparent in this measurement set, which offers an even distribution of measurements across polygon types. At this time, decomposition of old carbon consistently dominated the respiration flux from HC polygon centers ($\Delta^{14}C_{Reco} = -51.6 \pm 32.4\,‰$), whereas fast-cycling pools dominated respiration from FC and LC polygon centers (13.0 ± 10.9 and $5.9 \pm 5.6\,‰$, respectively; Fig. 3c). Ecosystem respiration rates were comparable across the three polygon types (Fig. 3b), which indicates that absolute rates of old carbon

decomposition were greater from HC polygons than from LC or FC polygons. The spatial pattern in old carbon decomposition was not tightly linked to $\Delta^{14}C_{SOC}$, which was ^{14}C-depleted relative to the respiration flux in both shallow and deep samples (Fig. 3c, d, Tables S1, S2). Differences in ^{14}C between bulk soil carbon and the respired fraction are commonly observed across ecosystems and soils, as soil carbon is comprised of components with a range of cycling rates (Dioumaeva et al., 2002; Hicks Pries et al., 2013; Schuur and Trumbore, 2006; Trumbore, 2000). Additionally, spatial and temporal variations in autotrophic respiration obscure relationships between soil-respired CO_2 and ecosystem respiration.

We saw no correlation in September 2014 between $\Delta^{14}C_{Reco}$ and thaw depth, which was greatest at this time in FC polygons (Fig. 3a). In contrast, repeated measurements from individual soil locations showed a general decrease in $\Delta^{14}C_{Reco}$ as thaw depth increased and exposed deeper soil layers to unfrozen conditions (Table S1). These findings suggest that the relationship between the depth of thaw and old carbon mineralization depends on the spatial and temporal scales of observation. At the scale of an individual soil profile, seasonal variations in $\Delta^{14}C_{Reco}$ correspond with changes in thaw depth. $\Delta^{14}C$ of soil organic matter tends to increase with depth in the soil, particularly in permafrost environments where the brevity of summer thaw strongly limits carbon turnover at depth (Hicks Pries et al., 2013; McFarlane et al., 2013; Torn et al., 2002; Trumbore, 2000; Fig. 3d). Accordingly, increasingly ^{14}C-depleted soil organic matter becomes available to decomposers as soil thaw deepens over the summer season. At the site scale, however, thaw depth may not be a useful predictor of spatial variations in $\Delta^{14}C_{Reco}$. Other differences – including variations in soil temperature profiles, organic layer thickness, vegetation productivity and rooting depth, the presence of cryoturbation, and oxygen availability to decomposers (Newman et al., 2015; Ping et al., 2015; Sloan et al., 2014; Vaughn et al., 2016) – may lead to microtopographic differences in the shape of $\Delta^{14}C_{SOC}$ depth profiles and the relative contributions of different carbon source pools to the decomposition flux.

In July and September 2013 and September 2014, ecosystem respiration ranged between 0.32 and $2.5\,\mu mol\,CO_2\,m^{-2}\,s^{-1}$ (Fig. 4). The relationship between the rate and radiocarbon content of ecosystem respiration was highly variable, but with two notable patterns across all data. First, as ecosystem respiration increased, the variance of $\Delta^{14}C_{Reco}$ tended to decrease. Second, there were no negative $\Delta^{14}C_{Reco}$ measurements associated with fluxes above $1\,\mu mol\,CO_2\,m^{-2}\,d^{-1}$ (Fig. 4). These patterns reflect the sensitivity of ecosystem respiration to the most dynamic carbon sources, autotrophic respiration and shallow soil carbon mineralization. Autotrophic respiration can contribute as much as 70 % of ecosystem respiration at the peak of the growing season (Hicks Pries et al., 2013), de-
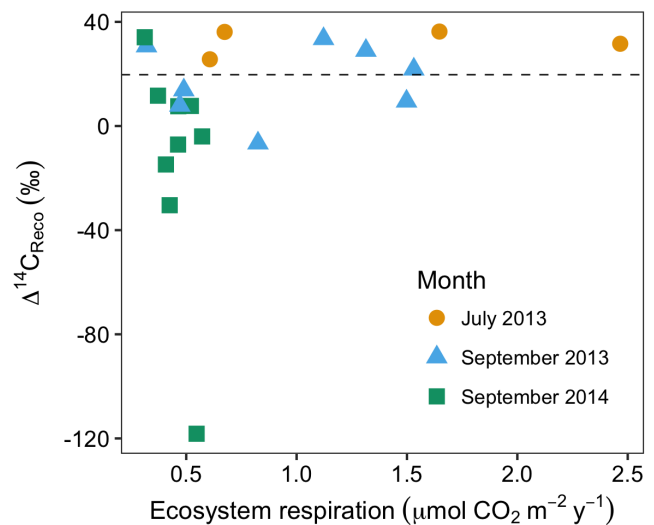

Figure 4. Rates and radiocarbon contents of ecosystem respiration in July and September 2013 and September 2014. The dashed horizontal line indicates the mean $\Delta^{14}C$ of local atmospheric CO_2 during the 2013 and 2014 summer seasons.

clining markedly as plants senesce. Similarly, heterotrophic decomposition rates are both highest and most temporally variable in shallow soil layers (Hicks Pries et al., 2013), where soil temperatures exhibit a large seasonal range. Supporting our interpretation, previous studies documenting seasonal variations in CO_2 exchange at this site (Oechel et al., 1995; Vaughn et al., 2016; Zona et al., 2014) indicate that ecosystem respiration, gross primary production, and soil surface temperatures peak in July or August, then decline into the late summer and fall. During the early summer period when respiration fluxes are high, high rates of autotrophic respiration and shallow soil respiration dominate the overall respiration flux. As a result, old, slow-cycling carbon respired from deep soils comprises a large percentage of ecosystem respiration only when respiration rates are low from autotrophic and shallow (fast-cycling) soil sources.

5.2 Radiocarbon in soil pore-space CO_2

At a subset of locations and sampling dates, we measured the radiocarbon content of CO_2 in soil pore gas ($\Delta^{14}C_{CO_2p}$). $\Delta^{14}C_{CO_2p}$ varied widely among profiles and sampling dates from −7.1 to −280‰ (Table 1, Fig. 5). These consistently negative values indicate that pore-space CO_2 was derived primarily from older soil organic matter, with minimal contributions from plant-respired carbon or fast-cycling soil organic carbon. In contrast, ecosystem respiration was generally enriched in radiocarbon relative to soil pore-space CO_2, even at only 10 cm depth (Fig. 5). This observation suggests that although old, slow-cycling carbon dominates soil pore-space CO_2, the shallowest CO_2 sources – autotrophic respiration and/or heterotrophic decomposition of fast-cycling (annual-

Table 1. Isotopic composition of soil profile CO$_2$.

Profile	Sampling date	Depth (cm)	$\delta^{13}C_{CO_2}$ (‰)	^{14}C analysis year	^{14}C sample size (mg C)	$F^{14}C$	$\Delta^{14}C_{CO_2}$ (‰)	Mean age of respired C (years)
HC1-center	8/2012	31	–	2013	0.044	0.7464	−259.2 ± 7.5	3050
HC1-center	9/2013	20	−23.7	2013	0.94	0.7270	−278.6 ± 2.6	3350
HC3-center	8/2012	10	−20.1	2013	0.29	0.9473	−59.9 ± 3.0	770
	8/2012	20	–	2013	0.37	0.8864	−120.3 ± 3.2	1320
	8/2012	29	−21.7	2013	0.46	0.8944	−112.4 ± 2.7	1240
HC3-center	7/2013	10	–	2013	0.12	0.9037	−101.3 ± 4.4	1150
	7/2013	20	–	2013	0.14	0.7382	−267.4 ± 2.6	3170
HC3-trough	7/2013	10	–	2013	0.19	0.7898	−216.2 ± 3.3	2440
	7/2013	20	−23.7	2013	0.83	0.8447	−161.7 ± 2.4	1760
FC2-center	8/2012	10	−24.8	2013	1.44	0.9509	−56.3 ± 2.8	740
	8/2012	20	−24.9	2013	1.35	0.9729	−34.5 ± 2.9	580
FC4-center	7/2013	20	−24.8	2013	0.99	0.8034	−202.7 ± 2.1	2260
LC3-trough	7/2013	10	−24.7	2013	0.72	1.0005	−7.1 ± 3.9	410
	7/2013	20	–	2013	0.16	0.8755	−131.2 ± 3.7	1430

decadal) organic carbon – contribute large proportions of the total respiration flux, even late in the season when plants have largely senesced. Detecting and characterizing the decomposition of older, deeper soil organic carbon requires direct measurements of soil pore-space CO$_2$. Such measurements provide a qualitative indicator of old carbon decomposition; as with surface CO$_2$ effluxes, proportional or absolute contributions from distinct carbon pools cannot be calculated without well-resolved vertical distributions of ^{14}C and ^{13}C source pools, as well as gas transport rates within the profile.

In most soil profiles, $\Delta^{14}C_{CO_2p}$ became increasingly negative with depth in the soil. This depth trend is similar to that seen in $\Delta^{14}C_{SOC}$ profiles measured from this site (Fig. 3d, Table S2), indicating that the cycling rates of both bulk soil organic matter and the decomposing carbon fraction tend to decrease with depth in the soil. Because frozen or near-freezing temperatures slow decomposition from the deep active layer throughout the majority of summer, this pattern is what would be expected in the absence of vertical mixing or rapid contributions of fast-cycling carbon at depth. In contrast with this general trend, soil pore-space CO$_2$ from three soil profiles (HC3-trough, HC3-center, and FC2-center) became enriched in radiocarbon near the permafrost table (Fig. 5, Table 1), a pattern that has been previously observed in the Arctic (Lupascu et al., 2014a). In these three profiles, concentrations of CO$_2$ in deep pore-space samples were 6 to 25 times higher than background atmosphere, so we infer that the higher $\Delta^{14}C_{CO_2p}$ values at depth were not caused by downward transport of atmospheric CO$_2$. Instead, this observation indicates significant CO$_2$ production from fast-

cycling carbon near the permafrost table. As in other Arctic sites, this depth trend is likely due either to cryoturbation (Bockheim and Tarnocai, 1998) or DOC leaching (Lupascu et al., 2014a), both of which can transport recently fixed, relatively decomposable carbon to the deep section of the active layer.

With $\Delta^{14}C_{CO_2p}$ values, we used a single pool turnover time model to calculate the mean age of pore-space CO$_2$ (Table 1). This model assumes that CO$_2$ is respired from a homogeneous pool of decomposing carbon (Trumbore, 2000) such that the turnover time equals the mean age of the respired carbon (Sierra et al., 2017). Across all measurement dates and depths, we found the mean age of respired CO$_2$ ranged from 410 years in one 10 cm sample to 3350 years at only 20 cm depth, indicating decomposition of old and/or slow-cycling carbon, even in relatively shallow soils. HC polygon centers produced particularly old CO$_2$, with ages greater than 3000 years from HC3-center in July 2013 and HC1-center in August 2012 and September 2013. This observation aligns with the spatial patterns we observed in surface CO$_2$ emissions, which were particularly ^{14}C-depleted in HC polygons (Fig. 2, Table S1). Together, these findings suggest that low $\Delta^{14}C_{Reco}$ from HC polygon centers was due to mineralization of very old carbon at depth. Because of unknown diffusion rates within the soil profile, it is challenging to quantitatively use pore-space CO$_2$ measurements to link soil carbon cycling rates to soil surface $\Delta^{14}C_{Reco}$. Low diffusion rates can lead to the accumulation of high concentrations of ^{14}C-depleted, slow-cycling CO$_2$ deep in the soil profile (Lee et al., 2010), and vertical mixing can transport
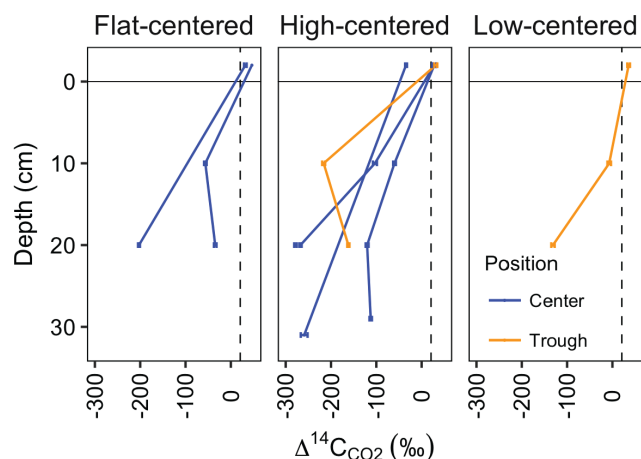
Figure 5. Soil depth profiles of Δ^{14}C-CO$_2$. Lines connect samples collected in the same vertical profile and month, and error bars represent analytical error. Values at -2 cm depth represent samples collected from surface soil chambers and reflect CO$_2$ that accumulated after chambers were scrubbed of CO$_2$. All other samples were collected from subsurface soil probes. Dashed vertical line indicates the mean Δ^{14}C of local atmospheric CO$_2$ during the 2012 and 2013 summer seasons.

CO$_2$ away from the site of production prior to its collection as soil pore gas.

Our findings of consistently negative Δ^{14}C values from soil pore-space CO$_2$ are similar to those from the other Arctic sites where it has been measured (Czimczik and Welker, 2010; Lupascu et al., 2014b, a). In contrast, studies in temperate or tropical sites find Δ^{14}C$_{CO2p}$ values that are more similar to atmospheric values (Borken et al., 2006; Gaudinski et al., 2000; Trumbore, 2000), where soil respiration is dominated by root respiration and decomposition of rapidly cycling soil organic matter. This difference may be due in part to differences among biomes in rooting distributions. Because of strong vertical gradients in soil temperature and nutrient and water availability, rooting distributions in Arctic tundra are extremely shallow (Iversen et al., 2015), limiting most root respiration to the shallow organic layer. Additionally, such negative Δ^{14}C$_{CO2p}$ values suggest that old, slow-cycling organic matter in Arctic soils is readily decomposable under thawed conditions. Cold soil temperatures and frozen conditions limit microbial activity throughout much of the year, allowing otherwise-decomposable soil organic matter to accumulate. During the short season in which Arctic soils are thawed, these large pools of ^{14}C-depleted soil carbon may be largely unprotected against microbial mineralization. Compared with tropical or temperate soils, existing Arctic soil carbon stores may thus be particularly vulnerable to warming.

Due to sampling limitations, ^{14}C data from soil pore-space CO$_2$ are available from only a subset of polygon types, positions, sampling dates, and depths. No samples were collected from polygon rims, and only few samples were obtained where soils were saturated (Table 1). For this reason, our dataset does not capture the full range of microtopographic variations in deep soil decomposition rates and controls. Soil temperature profiles, soil pore-space oxygen availability, soil organic matter concentration and chemistry, and vegetation composition, rooting distribution, and productivity influence microbial activity and vary among profiles and with time in the thawed season (Lipson et al., 2012; Olivas et al., 2011). In particular, these controls on decomposition dynamics likely differ between saturated and unsaturated soils, due both to the direct effects of saturation and to covarying effects of microtopography. For this reason, radiocarbon values presented in this manuscript cannot be scaled across the full range of environmental variation present at the site. To better characterize the relationships between these variables and soil carbon decomposition rates, further measurements are needed of ^{14}C in soil pore-space DIC and CO$_2$, across spatial, seasonal, and hydrological gradients.

6 Data availability

Data are stored in the Next-Generation Ecosystem Experiments (NGEE-Arctic) data repository (Vaughn et al., 2018; Vaughn and Torn, 2018) and may be accessed at http://dx.doi.org/10.5440/1364062 and https://doi.org/10.5440/1418853. The code used to generate plots and correct chamber samples for atmospheric contamination can be found at https://github.com/lydiajsvaughn/Radiocarbon_field_Barrow. The code used for turnover time modeling can be found at https://github.com/lydiajsvaughn/Radiocarbon_inc_2012.

7 Conclusions

We measured the radiocarbon contents of ecosystem respiration and soil pore-space CO$_2$ between 2012 and 2014 in Utqiaġvik, Alaska. As a naturally occurring tracer of soil carbon dynamics, radiocarbon in CO$_2$ and soil carbon reflects the rates at which carbon cycles through plant and soil pools (Trumbore, 2000). Radiocarbon provides a powerful tool to test and parameterize bottom-up models of the carbon cycle (He et al., 2016), constrain source signatures in inverse modeling studies (Randerson et al., 2002), and evaluate how environmental variables, seasonal changes, and disturbance influence decomposition rates from fast- and slow-cycling carbon pools. In Arctic sites, where cycling rates can be very slow, radiocarbon can be used to detect changes in decomposition from millennial-cycling pools (Hicks Pries et al., 2013; Schuur et al., 2009), which strongly influence long-term carbon dynamics but may be impossible to detect with other methods. Only limited data are available of radiocarbon in ecosystem respiration or soil pore-space CO$_2$, particularly from Arctic sites where samples can be difficult to obtain due to low rates of CO$_2$ production. To characterize seasonal

and spatial variations in the age of carbon pools contributing to total CO_2 efflux, we measured radiocarbon in ecosystem respiration and soil pore-space CO_2 across three summer seasons in Arctic polygon tundra.

$\Delta^{14}C$ in ecosystem respiration varied between $+60.5$ and $-160\,‰$ across the 3 years, with a strong seasonal trend (Fig. 2). July and August $\Delta^{14}C_{Reco}$ measurements were generally close to the $\Delta^{14}CO_2$ values of the local atmosphere, which declined from $22.2\,‰$ in 2012 to $17.7\,‰$ in 2014. In September, in contrast, over half the $\Delta^{14}CO_2$ measurements differed greatly from the local atmosphere (Fig. 2), contributing ^{14}C-depleted CO_2 to the atmospheric pool. These seasonal variations in $\Delta^{14}C_{Reco}$ and respiration rates contribute to the strong seasonal cycles of atmospheric $\Delta^{14}CO_2$ observed in the high latitudes (Graven et al., 2012). By quantifying these variations – respiration flux rates and radiocarbon values over space and time – this dataset offers useful information for atmospheric budgeting and inversions.

Measurements of radiocarbon in late-season ecosystem respiration indicate that carbon that cycles on millennial timescales contributes substantially to soil respiration. When thaw depth approached its maximum in September and October, highly depleted ^{14}C in respiration indicated that carbon older than 1000 years was a major source of heterotrophic respiration. Decomposition of old, slow-cycling soil carbon, however, may be missed when measuring surface $\Delta^{14}C_{Reco}$ alone. In the soil pore space, $\Delta^{14}C_{CO_2p}$ declined steeply with depth, particularly in high-centered polygons (Fig. 4); at only 20 cm below the soil surface, the mean age of carbon in the decomposition flux was as old as 3000 years (Table 1). Together, these observations suggest that during the short summer thaw season, ancient carbon stores in the deep active layer become available to decomposition, stabilized otherwise by cold, often frozen, and often anaerobic conditions (Mikan et al., 2002; Schmidt et al., 2011; Schuur et al., 2015).

As climate change alters these environmental controls and soils warm and thaw, a key question is how decomposition rates will change. Where permafrost degradation occurs, either through gradual deepening of the active layer or rapid thaw events, old soil carbon that has remained frozen for years to millennia is exposed to thawed conditions. A particularly important – but unknown – factor is the decomposition rate of this carbon released from thawing permafrost (Hicks Pries et al., 2013; Koven et al., 2015; Kuhry et al., 2013). Our measurements cannot differentiate between such newly thawed soil organic matter and carbon that has historically experienced an annual thaw. Our data do show, however, that when it is unfrozen, even very old Arctic soil organic carbon will readily decompose. As thaw depth progressed to the permafrost boundary, we consistently documented CO_2 production via decomposition of centennial carbon pools. As permafrost thaw progresses and Arctic soils warm, further measurements of soil-respired $^{14}CO_2$ across spatial and temporal gradients will provide critical information on soil carbon vulnerability.

Edited by: Kirsten Elger
Reviewed by: two anonymous referees

References

ACIA: Impacts of a Warming Arctic: Arctic Climate Impact Assessment, Cambridge University Press, Cambridge, UK, available at: https://www.amap.no/documents/doc/impacts-of-a-warming-arctic-2004/786 (last access: 27 September 2018), 2004.

Baldocchi, D.: 'Breathing' of the terrestrial biosphere: lessons learned from a global network of carbon dioxide flux measurement systems, Aust. J. Bot., 56, 1–26, https://doi.org/10.1071/BT07151, 2008.

Billings, W. D. and Peterson, K. M.: Vegetational change and ice-wedge polygons through the thaw-lake cycle in Arctic Alaska, Arctic Alpine Res., 12, 413–432, 1980.

Black, R. F.: Gubik Formation of Quaternary age in northern Alaska, United States Geological Survey, available at: http://pubs.er.usgs.gov/publication/pp302C (last access: 29 July 2014), 1964.

Bockheim, J. G. and Tarnocai, C.: Recognition of cryoturbation for classifying permafrost-affected soils, Geoderma, 81, 281–293, https://doi.org/10.1016/S0016-7061(97)00115-8, 1998.

Bockheim, J. G., Everett, L. R., Hinkel, K. M., Nelson, F. E., and Brown, J.: Soil organic carbon storage and distribution in Arctic tundra, Barrow, Alaska, Soil Sci. Soc. Am. J., 63, 934–940, 1999.

Bond-Lamberty, B. and Thomson, A.: A global database of soil respiration data, Biogeosciences, 7, 1915–1926, https://doi.org/10.5194/bg-7-1915-2010, 2010.

Borken, W., Savage, K., Davidson, E. A., and Trumbore, S. E.: Effects of experimental drought on soil respiration and radiocarbon

efflux from a temperate forest soil, Glob. Change Biol., 12, 177–193, https://doi.org/10.1111/j.1365-2486.2005.001058.x, 2006.

Brown, J., Miller, P. C., Tieszen, L. L., and Bunnell, F.: An Arctic ecosystem?: the coastal tundra at Barrow, Alaska, Dowden, Hutchinson and Ross, Inc., Stroudsburg, Pennsylvania, available at: https://darchive.mblwhoilibrary.org/handle/1912/222 (last access: 30 March 2014), 1980.

Bubier, J., Crill, P., and Mosedale, A.: Net ecosystem CO_2 exchange measured by autochambers during the snow-covered season at a temperate peatland, Hydrol. Process., 16, 3667–3682, https://doi.org/10.1002/hyp.1233, 2002.

Chapin III, F. S., Tieszen, L. L., Lewis, M. C., Miller, P. C., and McCown, B. H.: Control of tundra plant allocation patterns and growth, in: An Arctic Ecosystem: The Coastal Tundra at Barrow, Alaska, edited by: Brown, J., Miller, P. C., Tieszen, L. L., and Bunnell, F., Dowden Hutchinson Ross Stroudsburg Penn, 140–185, 1980.

Chasar, L. S., Chanton, J. P., Glaser, P. H., Siegel, D. I., and Rivers, J. S.: Radiocarbon and stable carbon isotopic evidence for transport and transformation of dissolved organic carbon, dissolved inorganic carbon, and CH_4 in a northern Minnesota peatland, Global Biogeochem. Cy., 14, 1095–1108, https://doi.org/10.1029/1999GB001221, 2000.

Czimczik, C. I. and Welker, J. M.: Radiocarbon Content of CO_2 Respired from High Arctic Tundra in Northwest Greenland, Arct. Antarct. Alp. Res., 42, 342–350, https://doi.org/10.1657/1938-4246-42.3.342, 2010.

Davidson, E. A., Savage, K., Verchot, L. V., and Navarro, R.: Minimizing artifacts and biases in chamber-based measurements of soil respiration, Agr. Forest Meteorol., 113, 21–37, https://doi.org/10.1016/S0168-1923(02)00100-4, 2002.

Dennis, J. G.: Distribution Patterns of Belowground Standing Crop in Arctic Tundra at Barrow, Alaska, Arctic Alpine Res., 9, 113–127, https://doi.org/10.2307/1550574, 1977.

Dioumaeva, I., Trumbore, S., Schuur, E. A. G., Goulden, M. L., Litvak, M., and Hirsch, A. I.: Decomposition of peat from upland boreal forest: Temperature dependence and sources of respired carbon, J. Geophys. Res., 107, 8222, https://doi.org/10.1029/2001JD000848, 2002.

Donner, N., Karpov, N. S., de Klerk, P., and Joosten, H.: Distribution, diversity, development and dynamics of polygon mires: examples from Northeast Yakutia (Siberia), available at: http://www.pimdeklerk-palynology.eu/polygon_mires_PI__Minke_et_al_2007_.pdf (last access: 27 September 2018), 2007.

Egan, J., Nickerson, N., Phillips, C., and Risk, D.: A Numerical Examination of $^{14}CO_2$ Chamber Methodologies for Sampling at the Soil Surface, Radiocarbon, 56, 1175–1188, https://doi.org/10.2458/56.17771, 2014.

Elberling, B., Michelsen, A., Schädel, C., Schuur, E. A. G., Christiansen, H. H., Berg, L., Tamstorf, M. P., and Sigsgaard, C.: Long-term CO2 production following permafrost thaw, Nat. Clim. Change, 3, 890–894, https://doi.org/10.1038/nclimate1955, 2013.

Gaudinski, J. B., Trumbore, S. E., Davidson, E. A., and Zheng, S.: Soil carbon cycling in a temperate forest: radiocarbon-based estimates of residence times, sequestration rates and partitioning of fluxes, Biogeochemistry, 51, 33–69, 2000.

Graven, H. D., Guilderson, T. P., and Keeling, R. F.: Observations of radiocarbon in CO_2 at seven global sampling sites in the Scripps flask network: Analysis of spatial gradients and seasonal cycles, J. Geophys. Res., 117, D02303, https://doi.org/10.1029/2011JD016535, 2012.

Hahn, V., Högberg, P., and Buchmann, N.: ^{14}C – a tool for separation of autotrophic and heterotrophic soil respiration, Glob. Change Biol., 12, 972–982, https://doi.org/10.1111/j.1365-2486.2006.001143.x, 2006.

Hardie, S. M. L., Garnett, M. H., Fallick, A. E., Ostle, N. J., and Rowland, A. P.: Bomb-^{14}C analysis of ecosystem respiration reveals that peatland vegetation facilitates release of old carbon, Geoderma, 153, 393–401, https://doi.org/10.1016/j.geoderma.2009.09.002, 2009.

He, Y., Trumbore, S. E., Torn, M. S., Harden, J. W., Vaughn, L. J. S., Allison, S. D., and Randerson, J. T.: Radiocarbon constraints imply reduced carbon uptake by soils during the 21st century, Science, 353, 1419–1424, https://doi.org/10.1126/science.aad4273, 2016.

Hicks Pries, C. E., Schuur, E. A. G., and Crummer, K. G.: Thawing permafrost increases old soil and autotrophic respiration in tundra: Partitioning ecosystem respiration using $\delta^{13}C$ and ^{14}C, Glob. Change Biol., 19, 649–661, https://doi.org/10.1111/gcb.12058, 2013.

Hinkel, K. M. and Nelson, F. E.: Spatial and temporal patterns of active layer thickness at Circumpolar Active Layer Monitoring (CALM) sites in northern Alaska, 1995–2000, J. Geophys. Res., 108, 8168, https://doi.org/10.1029/2001JD000927, 2003.

Hinkel, K. M., Paetzold, F., Nelson, F. E., and Bockheim, J. G.: Patterns of soil temperature and moisture in the active layer and upper permafrost at Barrow, Alaska: 1993–1999, Glob. Planet. Change, 29, 293–309, https://doi.org/10.1016/S0921-8181(01)00096-0, 2001.

Hopkins, F. M., Torn, M. S., and Trumbore, S. E.: Warming accelerates decomposition of decades-old carbon in forest soils, P. Natl. Acad. Sci. USA, 109, E1753–E1761, https://doi.org/10.1073/pnas.1120603109, 2012.

Hubbard, S. S., Gangodagamage, C., Dafflon, B., Wainwright, H., Peterson, J., Gusmeroli, A., Ulrich, C., Wu, Y., Wilson, C., Rowland, J., Tweedie, C., and Wullschleger, S. D.: Quantifying and relating land-surface and subsurface variability in permafrost environments using LiDAR and surface geophysical datasets, Hydrogeol. J., 21, 149–169, https://doi.org/10.1007/s10040-012-0939-y, 2013.

Hugelius, G., Strauss, J., Zubrzycki, S., Harden, J. W., Schuur, E. A. G., Ping, C.-L., Schirrmeister, L., Grosse, G., Michaelson, G. J., Koven, C. D., O'Donnell, J. A., Elberling, B., Mishra, U., Camill, P., Yu, Z., Palmtag, J., and Kuhry, P.: Estimated stocks of circumpolar permafrost carbon with quantified uncertainty ranges and identified data gaps, Biogeosciences, 11, 6573–6593, https://doi.org/10.5194/bg-11-6573-2014, 2014.

Iversen, C. M., Sloan, V. L., Sullivan, P. F., Euskirchen, E. S., McGuire, A. D., Norby, R. J., Walker, A. P., Warren, J. M., and Wullschleger, S. D.: The unseen iceberg: plant roots in arctic tundra, New Phytol., 205, 34–58, https://doi.org/10.1111/nph.13003, 2015.

Kaiser, C., Meyer, H., Biasi, C., Rusalimova, O., Barsukov, P., and Richter, A.: Conservation of soil organic matter through cryoturbation in arctic soils in Siberia, J. Geophys. Res., 112, G02017, https://doi.org/10.1029/2006JG000258, 2007.

Koven, C. D., Lawrence, D. M., and Riley, W. J.: Permafrost carbon-climate feedback is sensitive to deep soil carbon decomposability but not deep soil nitrogen dynamics, P. Natl. Acad. Sci. USA, 112, 3752–3757, https://doi.org/10.1073/pnas.1415123112, 2015.

Kuhry, P., Grosse, G., Harden, J. W., Hugelius, G., Koven, C. D., Ping, C.-L., Schirrmeister, L., and Tarnocai, C.: Characterisation of the Permafrost Carbon Pool, Permafrost Periglac., 24, 146–155, https://doi.org/10.1002/ppp.1782, 2013.

Lara, M. J., McGuire, A. D., Euskirchen, E. S., Tweedie, C. E., Hinkel, K. M., Skurikhin, A. N., Romanovsky, V. E., Grosse, G., Bolton, W. R., and Genet, H.: Polygonal tundra geomorphological change in response to warming alters future CO$_2$ and CH$_4$ flux on the Barrow Peninsula, Glob. Change Biol., 21, 1634–1651, https://doi.org/10.1111/gcb.12757, 2014.

Lee, H., Schuur, E. A. G., and Vogel, J. G.: Soil CO$_2$ production in upland tundra where permafrost is thawing, J. Geophys. Res., 115, G01009, https://doi.org/10.1029/2008JG000906, 2010.

Liljedahl, A. K., Boike, J., Daanen, R. P., Fedorov, A. N., Frost, G. V., Grosse, G., Hinzman, L. D., Iijma, Y., Jorgenson, J. C., Matveyeva, N., Necsoiu, M., Raynolds, M. K., Romanovsky, V. E., Schulla, J., Tape, K. D., Walker, D. A., Wilson, C. J., Yabuki, H., and Zona, D.: Pan-Arctic ice-wedge degradation in warming permafrost and its influence on tundra hydrology, Nat. Geosci., 9, 312–318, https://doi.org/10.1038/ngeo2674, 2016.

Lipson, D. A., Zona, D., Raab, T. K., Bozzolo, F., Mauritz, M., and Oechel, W. C.: Water-table height and microtopography control biogeochemical cycling in an Arctic coastal tundra ecosystem, Biogeosciences, 9, 577–591, https://doi.org/10.5194/bg-9-577-2012, 2012.

Loya, W. M., Johnson, L. C., Kling, G. W., King, J. Y., Reeburgh, W. S., and Nadelhoffer, K. J.: Pulse-labeling studies of carbon cycling in arctic tundra ecosystems: Contribution of photosynthates to soil organic matter, Global Biogeochem. Cy., 16, 1101, https://doi.org/10.1029/2001GB001464, 2002.

Lupascu, M., Welker, J. M., Xu, X., and Czimczik, C. I.: Rates and radiocarbon content of summer ecosystem respiration in response to long-term deeper snow in the High Arctic of NW Greenland, J. Geophys. Res.-Biogeosci., 119, 1180–1194, https://doi.org/10.1002/2013JG002494, 2014a.

Lupascu, M., Welker, J. M., Seibt, U., Xu, X., Velicogna, I., Lindsey, D. S., and Czimczik, C. I.: The amount and timing of precipitation control the magnitude, seasonality and sources (^{14}C) of ecosystem respiration in a polar semi-desert, northwestern Greenland, Biogeosciences, 11, 4289–4304, https://doi.org/10.5194/bg-11-4289-2014, 2014b.

McFarlane, K. J., Torn, M. S., Hanson, P. J., Porras, R. C., Swanston, C. W., Callaham, M. A., and Guilderson, T. P.: Comparison of soil organic matter dynamics at five temperate deciduous forests with physical fractionation and radiocarbon measurements, Biogeochemistry, 112, 457–476, https://doi.org/10.1007/s10533-012-9740-1, 2013.

Meijer, H. J., Pertuisot, M. H., and van der Plicht, J.: High-accuracy 614C measurements for atmospheric CO$_2$ samples by AMS, Radiocarbon, 48, 355–372, 2008.

Mikan, C. J., Schimel, J. P., and Doyle, A. P.: Temperature controls of microbial respiration in arctic tundra soils above and below freezing, Soil Biol. Biochem., 34, 1785–1795, 2002.

Mueller, C. W., Rethemeyer, J., Kao-Kniffin, J., Löppmann, S., Hinkel, K. M., and G. Bockheim, J.: Large amounts of labile organic carbon in permafrost soils of northern Alaska, Glob. Change Biol., 21, 2804–2817, https://doi.org/10.1111/gcb.12876, 2015.

Newman, B. D., Throckmorton, H. M., Graham, D. E., Gu, B., Hubbard, S. S., Liang, L., Wu, Y., Heikoop, J. M., Herndon, E. M., Phelps, T. J., Wilson, C. J., and Wullschleger, S. D.: Microtopographic and depth controls on active layer chemistry in Arctic polygonal ground, Geophys. Res. Lett., 42, 1808–1817, https://doi.org/10.1002/2014GL062804, 2015.

NOAA: National Weather Service Climate Services, available at: https://w2.weather.gov/climate/xmacis.php?wfo=pafg, last access: 9 October 2018.

Norman, J. M., Kucharik, C. J., Gower, S. T., Baldocchi, D. D., Crill, P. M., Rayment, M., Savage, K., and Striegl, R. G.: A comparison of six methods for measuring soil-surface carbon dioxide fluxes, J. Geophys. Res., 102, 28771–28777, https://doi.org/10.1029/97JD01440, 1997.

Nowinski, N. S., Taneva, L., Trumbore, S. E., and Welker, J. M.: Decomposition of old organic matter as a result of deeper active layers in a snow depth manipulation experiment, Oecologia, 163, 785–792, https://doi.org/10.1007/s00442-009-1556-x, 2010.

Nydal, R. and Lövseth, K.: Carbon-14 measurements in atmospheric CO2 from northern and southern hemisphere sites, 1962–1993, Oak Ridge National Lab., TN (United States), Oak Ridge Inst. for Science and Education, TN, USA, available at: http://www.osti.gov/scitech/biblio/461185 (last access: 24 May 2017), 1996.

Oechel, W. C., Vourlitis, G. L., Hastings, S. J., and Bochkarev, S. A.: Change in Arctic CO$_2$ Flux Over Two Decades: Effects of Climate Change at Barrow, Alaska, Ecol. Appl., 5, 846–855, https://doi.org/10.2307/1941992, 1995.

Oechel, W. C., Vourlitis, G., and Hastings, S. J.: Cold season CO$_2$ emission from Arctic soils, Global Biogeochem. Cy., 11, 163–172, https://doi.org/10.1029/96GB03035, 1997.

Olivas, P. C., Oberbauer, S. F., Tweedie, C., Oechel, W. C., Lin, D., and Kuchy, A.: Effects of Fine-Scale Topography on CO$_2$ Flux Components of Alaskan Coastal Plain Tundra: Response to Contrasting Growing Seasons, Arct. Antarct. Alp. Res., 43, 256–266, https://doi.org/10.1657/1938-4246-43.2.256, 2011.

Phillips, C. L., McFarlane, K. J., LaFranchi, B., Desai, A. R., Miller, J. B., and Lehman, S. J.: Observations of ^{14}CO$_2$ in ecosystem respiration from a temperate deciduous forest in Northern Wisconsin, J. Geophys. Res.-Biogeosci., 120, 600–616, https://doi.org/10.1002/2014JG002808, 2015.

Phillips, D. L. and Gregg, J. W.: Uncertainty in source partitioning using stable isotopes, Oecologia, 127, 171–179, https://doi.org/10.1007/s004420000578, 2001.

Ping, C. L., Bockheim, J. G., Kimble, J. M., Michaelson, G. J., and Walker, D. A.: Characteristics of cryogenic soils along a latitudinal transect in Arctic Alaska, J. Geophys. Res., 103, 28917–28928, 1998.

Ping, C. L., Jastrow, J. D., Jorgenson, M. T., Michaelson, G. J., and Shur, Y. L.: Permafrost soils and carbon cycling, SOIL, 1, 147–171, https://doi.org/10.5194/soil-1-147-2015, 2015.

Randerson, J. T., Enting, I. G., Schuur, E. A. G., Caldeira, K., and Fung, I. Y.: Seasonal and latitudinal variability of troposphere $\Delta^{14}CO_2$: Post bomb contributions from fossil fuels, oceans, the stratosphere, and the terrestrial biosphere: seasonal and latitudinal variability of trophosphere $\Delta^{14}CO_2$, Global Biogeochem. Cy., 16, 1112, https://doi.org/10.1029/2002GB001876, 2002.

Raz-Yaseef, N., Torn, M. S., Wu, Y., Billesbach, D. P., Liljedahl, A. K., Kneafsey, T. J., Romanovsky, V. E., Cook, D. R., and Wullschleger, S. D.: Large CO_2 and CH_4 emissions from polygonal tundra during spring thaw in northern Alaska, Geophys. Res. Lett., 44, 504–513, 2017.

Reimer, P. J., Bard, E., Bayliss, A., Beck, J. W., Blackwell, P. G., Ramsey, C. B., Buck, C. E., Cheng, H., Edwards, R. L., Friedrich, M., Grootes, P. M., Guilderson, T. P., Haflidason, H., Hajdas, I., Hatté, C., Heaton, T. J., Hoffmann, D. L., Hogg, A. G., Hughen, K. A., Kaiser, K. F., Kromer, B., Manning, S. W., Niu, M., Reimer, R. W., Richards, D. A., Scott, E. M., Southon, J. R., Staff, R. A., Turney, C. S. M., and van der Plicht, J.: IntCal13 and Marine13 Radiocarbon Age Calibration Curves 0–50,000 Years cal BP, Radiocarbon, 55, 1869–1887, https://doi.org/10.2458/azu_js_rc.55.16947, 2013.

Schmidt, M. W., Torn, M. S., Abiven, S., Dittmar, T., Guggenberger, G., Janssens, I. A., Kleber, M., Kögel-Knabner, I., Lehmann, J., and Manning, D. A.: Persistence of soil organic matter as an ecosystem property, Nature, 478, 49–56, 2011.

Schuur, E. A. G. and Trumbore, S. E.: Partitioning sources of soil respiration in boreal black spruce forest using radiocarbon, Glob. Change Biol., 12, 165–176, https://doi.org/10.1111/j.1365-2486.2005.01066.x, 2006.

Schuur, E. A. G., Vogel, J. G., Crummer, K. G., Lee, H., Sickman, J. O., and Osterkamp, T. E.: The effect of permafrost thaw on old carbon release and net carbon exchange from tundra, Nature, 459, 556–559, 2009.

Schuur, E. A. G., McGuire, A. D., Schädel, C., Grosse, G., Harden, J. W., Hayes, D. J., Hugelius, G., Koven, C. D., Kuhry, P., Lawrence, D. M., Natali, S. M., Olefeldt, D., Romanovsky, V. E., Schaefer, K., Turetsky, M. R., Treat, C. C., and Vonk, J. E.: Climate change and the permafrost carbon feedback, Nature, 520, 171–179, https://doi.org/10.1038/nature14338, 2015.

Shaver, G. R. and Billings, W. D.: Root Production and Root Turnover in a Wet Tundra Ecosystem, Barrow, Alaska, Ecology, 56, 401–409, https://doi.org/10.2307/1934970, 1975.

Shaver, G. R. and Kummerow, J.: Phenology, resource allocation, and growth of arctic vascular plants, in: Arctic Ecosystems in a Changing Climate an Ecophysiological Perspective, edited by: Chapin, F. S., Jefferies, R. L., Reynolds, J. F., and Shaver, G. R., Academic Press, Inc., San Diego, CA, 193–211, 1991.

Sierra, C. A., Müller, M., Metzler, H., Manzoni, S., and Trumbore, S. E.: The muddle of ages, turnover, transit, and residence times in the carbon cycle, Glob. Change Biol., 23, 1763–1773, 2017.

Sloan, V. L., Brooks, J. D., Wood, S. J., Liebig, J. A., Siegrist, J., Iversen, C. M., and Norby, R. J.: Plant community composition and vegetation height, Barrow, Alaska, Ver. 1, Carbon Dioxide Information Analysis Center, Oak Ridge National Laboratory, Oak Ridge, Tennessee, USA, https://doi.org/10.5440/1129476, 2014.

Strauss, J., Schirrmeister, L., Mangelsdorf, K., Eichhorn, L., Wetterich, S., and Herzschuh, U.: Organic-matter quality of deep permafrost carbon – a study from Arctic Siberia, Biogeosciences, 12, 2227–2245, https://doi.org/10.5194/bg-12-2227-2015, 2015.

Stuiver, M. and Polach, H. A.: Discussion reporting of ^{14}C data, Radiocarbon, 19, 355–363, 1977.

Torn, M.: CO2 CH4 flux Air temperature Soil temperature and Soil moisture, Barrow, Alaska 2013 ver. 1, Next Generation Ecosystems Experiment – Arctic, Oak Ridge National Laboratory (ORNL), Oak Ridge, TN, USA, 2015.

Torn, M. S., Lapenis, A. G., Timofeev, A., Fischer, M. L., Babikov, B. V., and Harden, J. W.: Organic carbon and carbon isotopes in modern and 100-year-old-soil archives of the Russian steppe, Glob. Change Biol., 8, 941–953, 2002.

Torn, M. S., Swanston, C. W., Castanha, C., and Trumbore, S. E.: Storage and turnover of organic matter in soil, in: Biophysico-Chemical Processes Involving Natural Nonliving Organic Matter in Environmental Systems, edited by: Senesi, N., Xing, B., and Huang, P. M., 219–272, https://doi.org/10.1002/9780470494950.ch6, 2009.

Trumbore, S.: Age of soil organic matter and soil respiration: radiocarbon constraints on belowground C dynamics, Ecol. Appl., 10, 399–411, 2000.

Trumbore, S.: Radiocarbon and soil carbon dynamics, Annu. Rev. Earth Pl. Sci., 37, 47–66, 2009.

Vaughn, L. J. S. and Torn, M. S: Radiocarbon in soil and CO_2 from laboratory incubation, Barrow, Alaska, 2014, Oak Ridge National Laboratory, Oak Ridge, Tennessee, USA, https://doi.org/10.5440/1418853, 2018.

Vaughn, L. J. S., Conrad, M. E., Bill, M., and Torn, M. S.: Isotopic insights into methane production, oxidation, and emissions in Arctic polygon tundra, Glob. Change Biol., 22, 3487–3502, https://doi.org/10.1111/gcb.13281, 2016.

Vaughn, L. J. S., Torn, M. S., Porras, R. C., Curtis, J. B., and Chafe, O.: Radiocarbon in Ecosystem Respiration and Soil Pore-Space CO_2 with Surface Gas Flux, Air Temperature, and Soil Temperature and Moisture, Barrow, Alaska, 2012–2014, Oak Ridge National Laboratory, U.S. Department of Energy, Oak Ridge, Tennessee, USA, https://doi.org/10.5440/1364062, 2018.

Wainwright, H. M., Dafflon, B., Smith, L. J., Hahn, M. S., Curtis, J. B., Wu, Y., Ulrich, C., Peterson, J. E., Torn, M. S., and Hubbard, S. S.: Identifying multiscale zonation and assessing the relative importance of polygon geomorphology on carbon fluxes in an Arctic Tundra Ecosystem, J. Geophys. Res. Biogeosci., 120, 788–808, https://doi.org/10.1002/2014JG002799, 2015.

Waldrop, M. P., Wickland, K. P., White III, R., Berhe, A. A., Harden, J. W., and Romanovsky, V. E.: Molecular investigations into a globally important carbon pool: Permafrost-protected carbon in Alaskan soils, Glob. Change Biol., 16, 2543–2554, 2010.

Xu, L. and Baldocchi, D. D.: Seasonal variation in carbon dioxide exchange over a Mediterranean annual grassland in California, Agr. Forest. Meteorol., 123, 79–96, https://doi.org/10.1016/j.agrformet.2003.10.004, 2004.

Xu, L., Furtaw, M. D., Madsen, R. A., Garcia, R. L., Anderson, D. J., and McDermitt, D. K.: On maintaining pressure equilibrium between a soil CO_2 flux chamber and the ambient air, J. Geophys. Res., 111, D08S10, https://doi.org/10.1029/2005JD006435, 2006.

Zona, D., Lipson, D. A., Zulueta, R. C., Oberbauer, S. F., and Oechel, W. C.: Microtopographic controls on ecosystem functioning in the Arctic Coastal Plain, J. Geophys. Res., 116, G00I08, https://doi.org/10.1029/2009JG001241, 2011.

Zona, D., Lipson, D. A., Richards, J. H., Phoenix, G. K., Liljedahl, A. K., Ueyama, M., Sturtevant, C. S., and Oechel, W. C.: Delayed responses of an Arctic ecosystem to an extreme summer: impacts on net ecosystem exchange and vegetation functioning, Biogeosciences, 11, 5877–5888, https://doi.org/10.5194/bg-11-5877-2014, 2014.

Zona, D., Gioli, B., Commane, R., Lindaas, J., Wofsy, S. C., Miller, C. E., Dinardo, S. J., Dengel, S., Sweeney, C., Karion, A., Chang, R. Y.-W., Henderson, J. M., Murphy, P. C., Goodrich, J. P., Moreaux, V., Liljedahl, A., Watts, J. D., Kimball, J. S., Lipson, D. A., and Oechel, W. C.: Cold season emissions dominate the Arctic tundra methane budget, P. Natl. Acad. Sci. USA, 113, 40–45, 2016.